Kinetics of Nucleation, Growth, and Stabilization of Cobalt Oxide Nanoclusters

S. King,[†] K. Hyunh,[‡] and R. Tannenbaum*,[†]

School of Materials Science and Engineering, Georgia Institute of Technology, Atlanta, Georgia 30332-0245, and Department of Chemical Engineering and Materials Science, University of Minnesota, Minneapolis, Minnesota 55455

Received: May 29, 2003; In Final Form: August 27, 2003

Metallic fragments, or metallomers (similar to the "mer"-based nomenclature for polymers), formed via the decomposition of organometallic complexes, are highly reactive, generating a nucleation and growth process that culminates in the formation of nanocrystals. In the absence of stabilizing molecules, the aggregation process is self-restricting mainly because of the decreasing mobility of the particles and their declining diffusional rates as a function of their increasing size. On the other hand, in the presence of a polymer in the reaction medium, the growing metallic particles are stabilized by the adsorption of the polymer chains onto their surfaces, thus lowering their surface energy and creating a barrier to further aggregation. Studies of the nucleation and aggregation kinetics of metallic particles formed from the decomposition of organometallic precursors have been used to shed light on the mechanism of their formation. In these studies, the rate of decomposition of the precursor organometallic complexes used has been deemed representative of the overall rate of the process. Moreover, it has implicitly been assumed that the formation kinetics of the metal nanoclusters directly mirrors the decomposition kinetics of the precursors. In this study, we attempt to decouple the kinetic characteristics of the various steps that comprise the overall nucleation and aggregation process for cobalt oxide nanoclusters. A combination of infrared and X-ray photoelectron spectroscopies, transmission electron microscopy, and dynamic light scattering is used to identify the individual contribution of each step to the overall mechanism of metal nanocluster formation.

1. Introduction

Understanding the molecular-level mechanisms responsible for the nucleation and aggregation of metal nanoclusters is essential in any process involving the self-assembly of hierarchical systems formed from metal nanocluster building blocks. Moreover, the physical and chemical properties of such metal nanoclusters are determined by their size, shape, and spatial distribution,[1−5] and hence, the ability to control these variables affords a high level of latitude in the design and fabrication of materials with nanoscale dimensions. This level of control of metal cluster nanostructure can be achieved through the proper choice of the synthesis and processing conditions. A synthesis method that is well suited for these requirements is the decomposition of organometallic complexes under controlled conditions in the presence of stabilizing molecules such as polymers to form stable, relatively uniform metal or metal oxide dispersions of very small particle size.[6−9] The overall reaction may be described as follows:

$$n\mathrm{M}_x(\mathrm{L})_y \xrightarrow[\text{energy, controlled atmosphere}]{\text{polymer, solvent}} \mathrm{M}_k^{(0)} \text{ and/or } (\mathrm{M}_j^{(i)}\mathrm{O}_{ij/2})_h + ny\mathrm{L}$$

(where M = metal, L = organic ligand, $k = nx$, and $h = nx/j$).

The energy-induced decomposition of these organometallic precursors is initiated by the loss of at least one ligand, followed by a cascade of ligand dissociation and complex rearrangements, giving rise to coordinatively unsaturated, multinuclear metal complexes having a higher metal/ligand ratio than the original precursor.[10−12] These metallic fragments, or metallomers (similar to the "mer"-based nomenclature for polymers), created by the energy-induced decomposition of organometallic complexes are highly reactive,[2,3] generating a nucleation and growth process that culminates in the formation of nanocrystals. In the absence of stabilizing molecules, the aggregation process is self-restricting mainly because of the decreasing mobility of the particles as a function of their increasing size and because of the declining diffusional rates of the larger metallic fragments achievable in the reaction medium. The reactivity of the coordinatively unsaturated organometallic species formed during the decomposition process, even at low precursor concentration, constitutes the driving force for the formation of the metallomers via van der Waals attraction forces, and hence, the nucleation process is not generated by supersaturation, as suggested by the LaMer mechanism.[13,14] The aggregation process, however, is strongly limited by the mobility and, consequently, by the diffusional rates of the growing particles, in accordance with both the LaMer mechanism and various growth models.[15−19]

On the other hand, in the presence of various reactive polymers in the reaction medium, that is, polymers having various functional groups, the growing metallic particles are stabilized by the adsorption of the polymer chains onto the surface of the growing metal fragments, lowering their surface energy and creating a barrier to further aggregation. Moreover, the increased solution viscosity due to the presence of even low concentrations of polymer has the effect of decreasing the

* Corresponding author. E-mail: rina.tannenbaum@mse.gatech.edu.
[†] Georgia Institute of Technology.
[‡] University of Minnesota.

10.1021/jp0355004 CCC: $25.00
Published on Web 10/15/2003

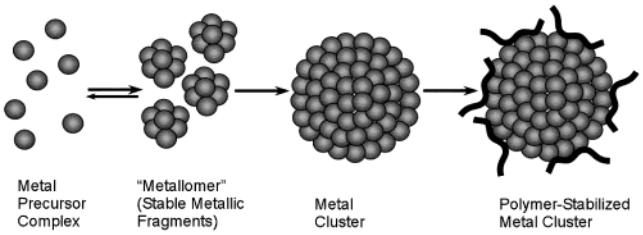

Figure 1. Schematic description of the formation of metallomers and the nucleation, growth, and stabilization of cobalt oxide nanoparticles.

diffusional rates of all species in the reaction solution,[20,21] thereby reducing the rates of both metallomer formation and metal nanocluster formation. The ability to control metal nanocluster size by manipulating their surface interactions with various polymer types, molecular weights, and concentrations[6,22] supports the presence of an autocatalytic surface-growth mechanism, such as that suggested by Finke et al.[23,24] The nucleation and growth of metal nanoclusters in such a case may be divided into three main steps (shown schematically in Figure 1): formation of stable metallomers under the experimental conditions, aggregation of the metallomers into larger fragments, the structure of which is defined by the presence of a large fraction of the metal atoms at the surface of the cluster, and finally, adsorption of the polymer chains onto the metal cluster surface, creating a stabilizing polymer layer capable of suppressing the van der Waals attraction forces between neighboring fragments.[25−27]

Hence, the steady-state size of the clusters formed is significantly influenced by the nature and molecular weight of the polymers. The type of functional groups and chain flexibility determine the strength of the interfacial interactions between the growing metal cluster and the adsorbed polymer layer. The nature of the interfacial bonding between the growing metal clusters and the polymer chains ranges from weak van der Waals forces to strong coordination or ionic bonds, depending on the metal and the functional groups of the polymer.[28,29] Because of their small size, the metal clusters exhibit high surface reactivity and ensure good mechanical coupling of the particles to the polymer matrix.[30−32]

The interactions between reactive metallomers and the surrounding polymer may occur via two different mechanisms: formation of a bond between a metallic center in a low-nuclearity cluster and the functional group (or groups) on the polymer chain, resulting in a polymer−metal complex, and adsorption of the polymer chains onto the surface of a high-nuclearity cluster via surface interactions. The first mechanism occurs primarily in systems in which the functional groups on the polymer react vigorously and irreversibly with the coordinatively unsaturated metallic species generated in the first stages of the decomposition reaction, and hence, it directly competes with the metal−metal aggregation process. In the second mechanism, the rates of the surface interactions between the polymer and the metallic cluster are slower than the metal−metal aggregation process, and they take place upon the formation of a pseudostable metallic aggregate. In a given system, both mechanisms occur simultaneously, but the relative dominance of one or the other is a function of the polymer reactivity (type of functional groups), polymer molecular weight (chain size), and type of metal precursor and its concentration.[9,20,27,28,31,33−38] The strength of the polymer interaction with the surface atoms in a cluster, that is, the permanence of the adhesive bond formed, and the effective thickness of the polymer layer bonded onto the surface, ultimately determine the equilibrium cluster size.

Studies of the nucleation and aggregation kinetics of metallic particles formed from the decomposition of organometallic precursors have been used to shed light on the mechanism of their formation. In these studies, the rate of decomposition of the precursor organometallic complexes used has been deemed representative of the overall rate of the process.[9,27] Moreover, it has implicitly been assumed that the formation kinetics of the metal nanoclusters directly mirrors the decomposition kinetics of the precursors. This assumption is due to the lack of direct experimental data with respect to the dynamics of metal cluster growth either in the absence or in the presence of polymers or any other stabilizing molecules.[25] Hence, information that may arise from the overlooked mismatch of the kinetics of the two processes has potentially a direct bearing on the elucidation of the mechanistic aspects of the nucleation and aggregation process as a whole.

In this study, we attempt to decouple the kinetic characteristics of the various steps that comprise the overall nucleation and aggregation process and identify the individual contribution of each step to the overall mechanism of metal nanocluster formation. The reaction chosen for this purpose is the formation of cobalt oxide particles by the thermal decomposition of $Co_2(CO)_8$ in the presence of poly(methyl methacrylate), PMMA, as the stabilizing agent. The decomposition of $Co_2(CO)_8$ in the presence of various polymers has been studied in detail by us and others,[39−41] but most of the attention has been concentrated on obtaining zerovalent nanoscale metallic particles under inert conditions. Unfortunately, such a system does not lend itself to the independent measurement of the kinetics of the metallic cobalt cluster formation, and hence, it cannot be used as the model system for kinetic decoupling. When the decomposition reaction is performed in an oxidative atmosphere, it will be possible to determine the independent rate of the formation of cobalt oxides and then compare it to the independent rate of the decomposition of the carbonyl complex. Moreover, when the changes that occur in the ester groups of the PMMA chains are followed, it will be possible to assess the kinetics of the adsorption of the polymer onto the cobalt oxide surface and reach some conclusions regarding the interim stages in the nucleation and growth process and the critical nanocluster sizes involved in each step of the overall process.

2. Experimental Method

2.1. Kinetic Analysis of the Oxidative Decomposition of $Co_2(CO)_8$. Five grams of PMMA pellets (Polyscience, Inc., $\bar{M}_w$ = 323 000) and 50 mL of chlorobenzene (Fisher-Reagent) were mixed for 48 h at room temperature in a 250 mL round-bottom flask. The chlorobenzene was dried using molecular sieve pellets. Fifty milliliters of a 5×10^{-2} M solution of $Co_2(CO)_8$ in chlorobenzene was added dropwise to the PMMA−chlorobenzene solution, and the resulting solution was mixed for 5 min. The solution was subsequently heated to 90 °C in an oxidative atmosphere (Air Products, 20% O_2, 78% N_2, and 2% H_2O vapor). The overall kinetics of the reaction was determined by removing aliquots of approximately 1 mL at different time intervals, quenching them with 4 mL of cold chlorobenzene and analyzing them by Fourier transform infrared spectroscopy. The infrared absorption band (measured on Nicolet MX-1 and Nicolet Nexus 870 Fourier transform infrared spectrophotometers) at 1858 cm^{-1} (bridging carbonyl stretching) was observed to change during decomposition of the cobalt-containing polymer solutions and was used to follow the kinetics of the

thermal decomposition reaction of $Co_2(CO)_8$. The absorption band at 886 cm^{-1}, corresponding to the stretching vibration of the Co−O bond in Co_2O_3, was used to monitor the formation of the cobalt oxide nanoclusters.

2.2. Preparation of PMMA-Coated Cobalt Oxide Nanocluster Samples. To extract measurable amounts of PMMA-coated cobalt oxide nanoclusters, several experiments, as those described in section 2.1., were performed. In each case, the reaction was stopped at a predetermined time (e.g., after 2 h, 5 h, etc.) by immersing the flask in an ice bath. The solution was divided into small portions (∼5 mL each) and placed in an Eppendorf Concentrator 5301 centrifuge (14 000 rpm). This separated excess solvent from the polymer-coated nanoclusters. The supernatant chlorobenzene solution was removed, and the remaining particles were washed with both chlorobenzene and hexane to remove any excess unbound polymer or partially reacted cobalt carbonyl fragments. The suspension was centrifuged again, and the process was repeated three times. The remaining wet paste was resuspended in a 5 mL, 10 wt % xylene solution of polyethylene (Aldrich, $\bar{M}_w \approx 125\,000$), and the suspension was allowed to mix well to obtain reasonable suspension homogeneity. Then the polymer suspension containing the PMMA-coated cobalt oxide nanoparticles was cast on three different substrates: (1) on a glass slide, (2) on a NaCl circular crystal, and (3) on a glass slide coated with 1000 Å of Ag. The film formed on the glass slide was analyzed by X-ray photoelectron spectroscopy (XPS), while the other two samples were analyzed by transmission FTIR and reflection−absorption FTIR, respectively.

2.3. Particle Size Determination. Samples for transmission electron microscopy (TEM) were prepared by depositing a drop of the reaction solution onto a Formvar coated copper TEM grid (Ted Pella). The grid rested on a thin piece of tissue, such that when the drop of solution was deposited on the grid, the tissue pulled the liquid through the grid, leaving a very thin film on the grid itself. Thin films were necessary for TEM imaging because electrons cannot penetrate thicker films. TEM analysis was done on both a JEOL 100CX TEM at an operating voltage of 100 keV and two high-resolution microscopes, a Hitachi HF-2000 and a JEOL 4000EX, both with operating voltages of 200 keV.

In parallel, dynamic light scattering (DLS) particle size determination was performed on 10 mL samples removed from the solutions prepared similarly to those described in section 2.2. The samples were placed in standard scintillation vials (∼27.4 mm diameter) as the sample cells. Measurements were conducted on a Brookhaven DLS system equipped with a 35 mW, 632.8 nm wavelength HeNe laser and a stepping motor allowing data collection at angle increments of 0.01°. The results were analyzed by using CONTIN, NNLS (nonnegative least squares), and Williams−Watts size distribution programs.

2.4. Surface-Sensitive Reflection−Absorption Infrared Spectroscopy (IRRAS). The preliminary infrared experiments on the samples with the Ag substrate were conducted on an IBM-IR-44 (Bruker) FTIR spectrometer equipped with a Harrick variable-angle specular reflection (IRRAS) attachment.[42] The cell chamber was purged with dry nitrogen for at least half an hour before collecting interferograms. The resolution was 2 cm^{-1}, and 3000 scans were collected for the bulk and the adsorbed polymer samples. Additional experiments were conducted on a Nicolet Nexus 870 equipped with a PM-IRRAS attachment. The polarization was achieved by using a 50 kHz ZnSe photoelastic modulator (PEM).[43] The polarization modulated IR light impinges on the sample surface near the grazing angle, ∼80°, and the reflected light from the sample surface is then collected by a BaF_2 lens and focused onto an MCT (cooled with liquid N_2) detector. Also in these experiments, the resolution was 2 cm^{-1}, and 3000 scans were collected for the bulk PMMA films and the adsorbed polyethylene samples containing the PMMA-coated cobalt oxide nanoclusters.

2.5. X-ray Photoelectron Spectroscopy (XPS). The X-ray photoelectron spectroscopy experiments were carried out using a Perkin-Elmer model 5400 spectrometer equipped with a UHV chamber using a double pass cylindrical mirror analyzer with nonmonochromatized Mg Kα (1253.6 eV) radiation and an analyzer pass energy of 35.75 eV. The source was operated at 100 W to minimize the damage to the PMMA films in the samples that were examined. Under these conditions, C(1*s*) spectra of bulk PMMA indicate that samples could be safely exposed to the source for about 15 min. The operating pressure of the vacuum chamber was 2×10^{-10} Torr. The measurements were made at 45° angle of incidence. The data analysis was carried out on a Perkin-Elmer 7000 computer.

3. Results and Discussion

The nucleation and growth of cobalt oxide nanoclusters formed by the decomposition of cobalt carbonyl complexes in the presence of an oxidative atmosphere may be divided into three main steps: (a) the formation of stable cobalt oxide nuclei under the experimental conditions, (b) the aggregation of the cobalt nuclei into larger oxide fragments the structure of which is defined by the presence of a large fraction of the oxide molecules at the surface of the cluster, and (c) the adsorption of the PMMA chains onto the oxide cluster surface, reducing the surface energy and limiting the growth of the particles. In previous studies, the rate of decomposition of the precursor organometallic complexes used in similar reactions has been deemed representative of the overall rate of the process. In this study, we attempt to deconvolute the kinetic characteristics of the various steps that comprise the overall process and identify the individual contribution of each step to the overall mechanism of cobalt oxide nanocluster formation.

The characterization of the cobalt oxide nanoparticle products, performed by both XRD and TEM diffraction patterns, shown in Figure 2, revealed that Co_2O_3 is the most abundant cobalt oxide found in the system. CoO is found as well, but even its highest intensity band, corresponding to the (111) crystal plane, was much less intense than the highest intensity band of Co_2O_3, as shown in Table 1. We are not ruling out the presence of Co_3O_4, but the intensity of the bands corresponding to this compound is relatively low, indicating a low concentration.

Figure 3 shows the kinetics of the decomposition and oxidation of $Co_2(CO)_8$ in a PMMA solution. The reaction is assumed to follow first-order kinetics. The decrease in the concentration of $Co_2(CO)_8$ is monitored by following the decrease of the 1858 and 1867 cm^{-1} absorption bands, corresponding to the stretching vibrational modes of the bridging carbonyls of the cobalt complex.[9,44−48] The 1858 cm^{-1} band is used as the analytic band. Because the intensity of this absorption band is directly proportional to the concentration of the cobalt complex in the polymer solution (via the relationship $E = \epsilon dc$), it is not necessary to engage in the lengthy process of calculating the molar extinction coefficient of $Co_2(CO)_8$ in the PMMA matrix, but it is sufficient to express the kinetic behavior as $\ln(E_{1858})$ vs time and extract the rate coefficient. The rate coefficient observed for this reaction is consistent with previous experiments conducted in similar circumstances in the presence of PMMA and other similar polymeric matrixes.

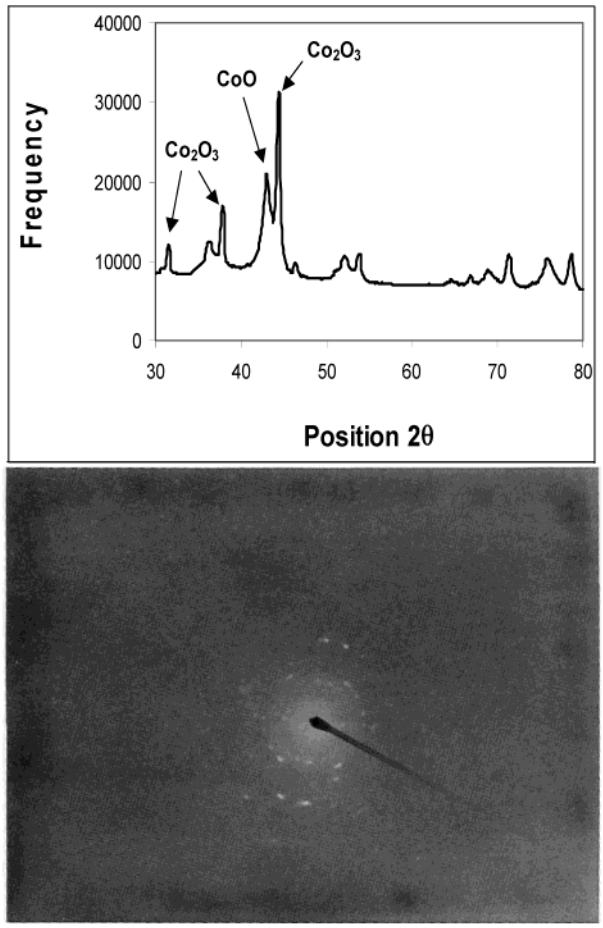

Figure 2. XRD (top) and TEM (bottom) diffraction patterns of the cobalt oxide nanocluster products obtained via the thermal decomposition of metal carbonyl precursors in the presence of PMMA and in an oxidative atmosphere.

TABLE 1: Analysis of the Diffraction Patterns of the Cobalt Oxide Nanoparticle Products Obtained from XRD and TEM Experiments

exptl XRD *d* spacing (Å)	exptl E-beam *d* spacing (Å)	cobalt oxide		exptl XRD relative intensity (%)
		Co_2O_3 *d* (Å)	CoO *d* (Å)	
3.326	3.210	3.321		14.3
2.901	2.970			14.9
2.799	2.817	2.836		32.9
2.484	2.481		2.460	52.7
2.405	2.330	2.380		100.0
2.315	2.324	2.320		6.8
2.105	2.163		2.130	5.2
2.075	2.024			13.1
2.017	1.960			15.1
1.712	1.852	1.780		6.1
1.662	1.630	1.645		10.9
1.572	1.576	1.570		20.0
1.492	1.472		1.506	14.8
1.450	1.379		1.397	15.8

Figure 4 shows the direct formation of the cobalt oxide clusters, as evidenced by the changes observed in the infrared absorption bands of the Co−O bonds in Co_2O_3 at 883 and 832 cm^{-1}, corresponding to the asymmetric and symmetric vibrational modes of the oxide, respectively.[49] The increase of the 883 cm^{-1} infrared absorption band, corresponding to the asymmetric Co−O stretch, is shown in Figure 4a. The plot of the absorption intensity of this band as a function of time is

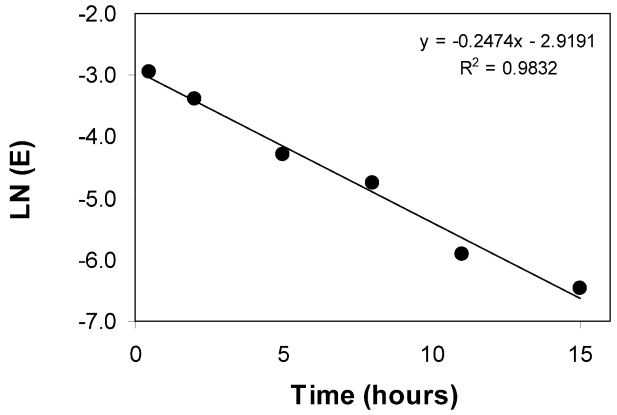

Figure 3. The kinetics of the decomposition and oxidation of $Co_2(CO)_8$ in a PMMA solution (as indicated by the changes in the intensity of the 1858 cm^{-1} infrared band). The rate coefficient is directly calculated from the plot of $\ln(E_{1858})$ vs time because the band intensity is directly proportional to the cobalt precursor concentration (via the relationship $E = \epsilon dc$).

compared to the plot of the absorption intensity of the 1858 cm^{-1} band as a function of time and shown in Figure 4b. It is interesting to note that the appearance of the 883 cm^{-1} infrared absorption band has an induction period, suggesting a delay in the formation of the oxide compared to the decrease in the concentration of the precursor. This suggests that the cobalt oxide nuclei are formed as a result of a reaction cascade in which the oxidation occurs only in the final step.[25] This, again, is consistent with various suggested mechanisms of cobalt carbonyl decompositions, in which the formation of stable nuclei is due to a systematic decrease in the CO/Co ratio,[11,50] generating coordinatively unsaturated and highly reactive cobalt species, which in turn undergo oxidation under ambient atmospheric conditions. An indication as to the critical size of cobalt fragments that are sufficient to generate the onset of the oxidation process can be assessed indirectly from the duration of the induction period. According to Figure 4b, at least in the first hour of the decomposition reaction, the intensity of the 1858 cm^{-1} band has decreased by ∼15% (that is, about 15% of the initial $Co_2(CO)_8$ has reacted) without generating a similar increase of the 883 cm^{-1} band. TEM micrographs and dynamic light scattering (DLS) measurements taken from samples generated during the induction period and at the end of the process (shown in Figure 4c on the left and right, respectively) show that no measurable particles were formed after 1 h of reaction, while the particles formed at the end of the process have an average size of ∼70 nm. Because the sensitivity limit of the DLS instrument is ∼3 nm, we conclude that the critical size for the onset of the oxidation of the cobalt reactive nuclei is ≤3 nm, that is, ≤860 cobalt atoms. Finally, the intensity of the 883 cm^{-1} infrared absorption band tapers off and reaches a plateau, suggesting a saturation of the cobalt oxide formation.

FTIR measurements of the washed cobalt oxide particles formed during the decomposition reaction, shown in Figure 5, reveal that an extensive reaction between the polymer and the metal oxide particles has taken place, resulting in the formation of $RCOO^-$ groups (where R is the PMMA main chain) and, hence, possibly a new $(RCOO^-)-Co^{III}$ complex. As the reaction progresses, three distinct functional groups on the PMMA are observed, (a) the initial C═O stretching vibration band at 1741 cm^{-1}, (b) the COOH stretching vibration at 1702 cm^{-1}, and the COO^- stretching vibration at 1674 cm^{-1}. The presence of these bands in the PMMA adsorbed onto the cobalt oxide particles points to the hydrolysis of the ester group of the PMMA

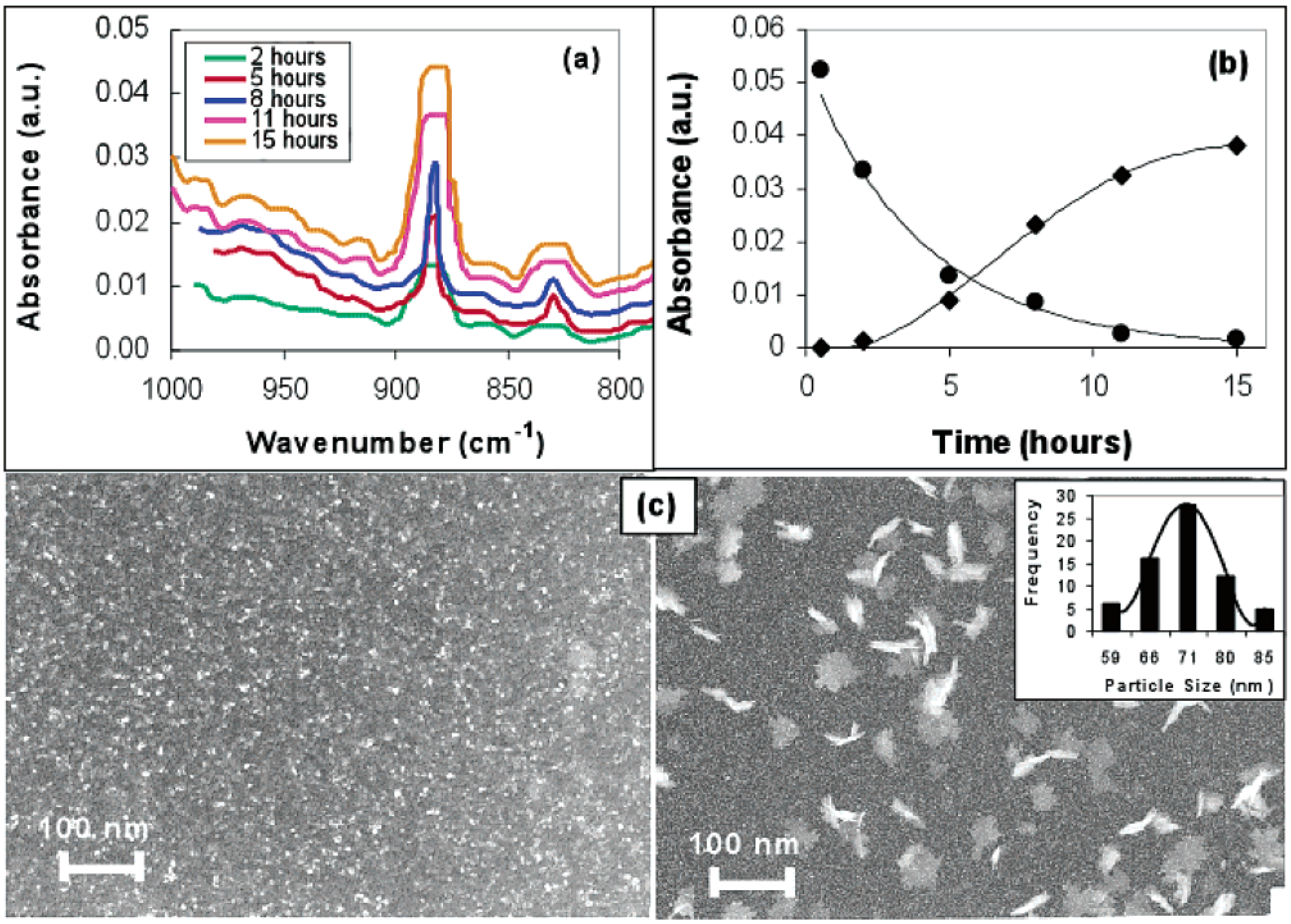

Figure 4. The direct formation of the cobalt oxide cluster as indicated by the appearance of the infrared absorption bands of the Co−O bonds in Co_2O_3 as a function of the growth of the cobalt oxide nanocluster: (a) the increase of the 852 cm^{-1} infrared absorption band corresponding to the Co−O stretch; (b) the plot of the absorption intensity of this band as a function of time compared to the plot of the absorption intensity of the 1858 cm^{-1} band as a function of time; (c) TEM micrographs and dynamic light scattering (DLS) measurements taken from samples generated during the induction period (left image) and at the end of the process (right image).

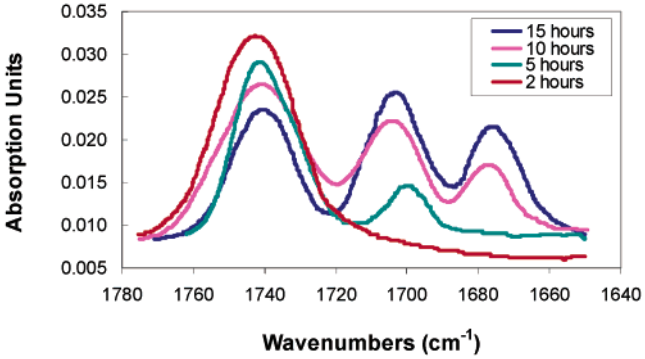

Figure 5. FTIR spectra of the washed cobalt oxide particles formed during the decomposition reaction and stabilized by PMMA.

with the subsequent formation of a carboxylic group followed by the formation of a carboxylate ion,[51−54] as shown:

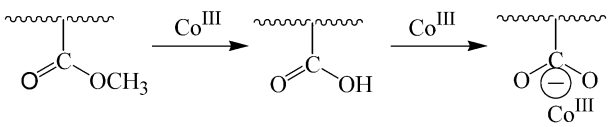

The methanol formed by this hydrolysis can diffuse through the thin PMMA film adsorbed on the surface of the oxide nanoparticles and slowly evaporate (bp 64.5 °C). Because the ester group resides on the side chain of the polymer, the hydrolysis of the ester bond does not result in chain scission.

The intensities of these three bands corresponding to the concentration of the three different functional groups on the adsorbed PMMA chains are shown in Figure 6a. During the induction period observed for the formation of cobalt oxide, no particles could be isolated, and hence, the first successful measurement was performed only after 2 h since the start of the reaction. Of particular interest is the delay in the appearance of the COO^- functional group because it is similar to the induction period observed in the formation of the oxide. Previous studies involving the reactive adsorption of PMMA on chromium oxide surfaces have shown that the PMMA chains adsorb onto the metal oxide surface via the direct ionic bonding of the carboxylate ion that was generated by the cleavage of the ester bond through hydrolysis, facilitated by the metal oxide surface.[54] As a result, the formation of the COO^- group is intimately linked to the formation of the cobalt oxide particles, and hence, the delay in the formation of the latter is mirrored in the formation of the former. Moreover, the formation of the carboxylate ion is initially slower than the formation of the carboxylic acid (i.e., the rate of the hydrolysis is greater than the dissociation of the newly formed COOH group), but the rate increases as the reaction proceeds. The relative intensities of the COOH band and the COO^- band expressed as the ratio of these bands with the C═O band are shown in Figure 6b. However, the overall rate of formation of the carboxylate ion

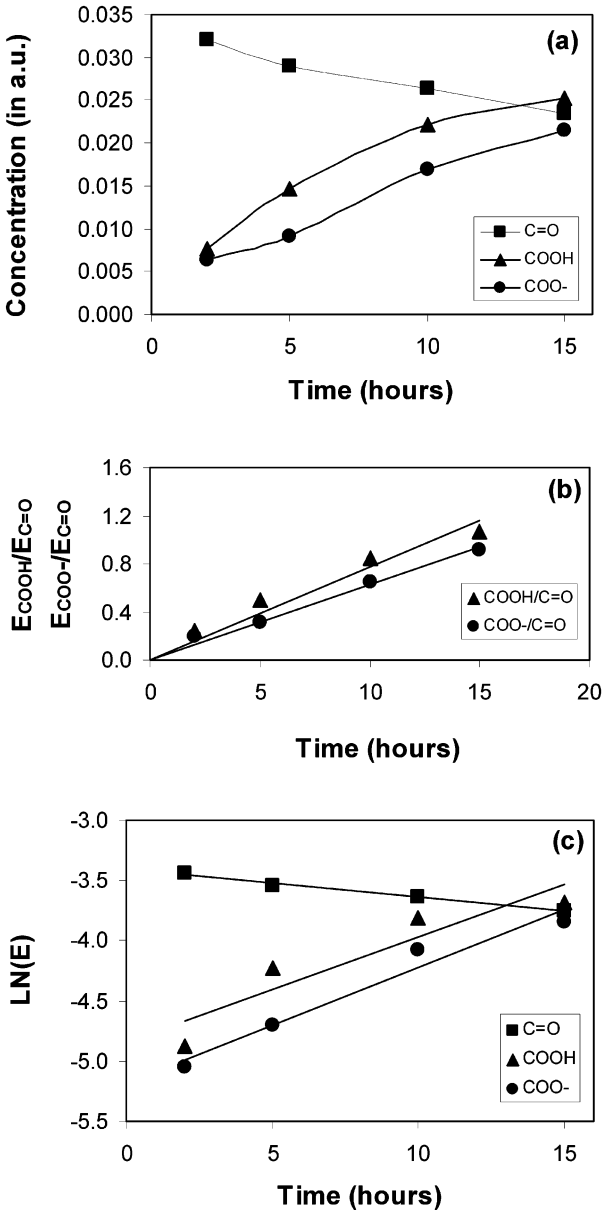

Figure 6. Comparison of the kinetics of the three functional groups formed during the reaction of PMMA with reactive cobalt oxide clusters: (a) plot of the three bands of interest, (■) the initial C═O stretching vibration band at 1741 cm^{-1}, (▲) the COOH stretching vibration at 1702 cm^{-1}, and (●) the COO^- stretching vibration at 1674 cm^{-1}; (b) plot of the relative intensities of (▲) the COOH band and (●) the COO− band expressed as the ratio of these bands with the C═O band; (c) plot of the overall rate of formation of the carboxylate ion compared to that of the formation of the COOH group.

is similar to that of the formation of the COOH group, as shown in Figure 6c. First-order formation rates are assumed, but because the overall reaction is composed of at least two consecutive reactions, this assumption may be only partially correct.

Further support for the hydrolysis mechanism of PMMA and the delayed formation of COO^- groups concurrent with the delayed formation of the cobalt oxide nanoparticles was obtained from XPS experiments. As a first step, the XPS spectra of a 250 Å PMMA film deposited by spin-coating on a polyethylene-coated glass substrate was considered for this study as bulk PMMA, and the precise position of the characteristic core C(1s) peaks was established, as shown in Table 2. Bulk PMMA gives rise to three C(1s) peaks (peak deconvolutions have been

TABLE 2: The Characteristic Core-Level C(1s) XPS Peaks of a 250 Å PMMA Film Deposited by Spin-Coating on a Polystyrene-on-Glass Substrate and Considered for This Study as Bulk PMMA[a]

Band No.	Peak Position (eV)	Delta (eV)	Peak Area (%)	Assignment of Atoms
3	288.69	4.12	13	
2	287.06	2.49	17	–O–$\underline{C}H_3$
1	284.57	0.00	67	aliphatic
4	287.94	3.37		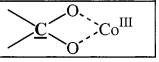

[a] The specific peaks are marked with identifying band numbers that appear in the text.

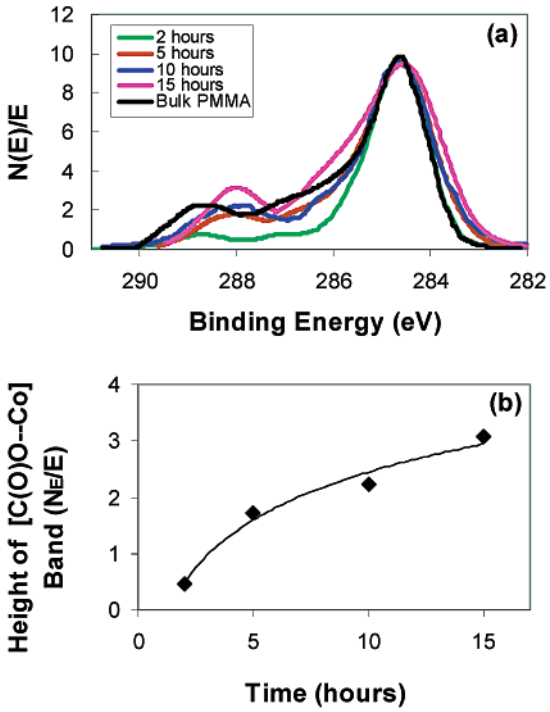

Figure 7. The high-resolution C(1s) core-level electron XPS contour spectra of the PMMA-stabilized cobalt oxide nanoparticles: (a) XPS spectra obtained at different reaction times and the contour spectrum of the bulk PMMA; (b) plot of the increase in the height of the 287.94 eV peak as a function of time.

performed but are not shown): (1) the 284.57 eV peak corresponds to the hydrocarbons in the main chain, (2) the 287.06 eV peak corresponds to the methyl group singly bonded to an oxygen atom, and (3) the 288.69 eV peak corresponds to the ester carbon.[55,56] The experimental ratios among these three peaks are 67:17:16, in reasonable agreement with the theoretical ratios of 3:1:1. Because the correct value for the binding energy of the C(1s) core electrons of a uncharged aliphatic hydrocarbon compound is 284.80 eV,[54−56] we conclude that there was no charging effect, which may take place when analyzing polymer films.[57]

The high-resolution C(1s) core-level electron contour XPS spectra of the PMMA-stabilized cobalt oxide nanoparticles obtained at different reaction times are shown in Figure 7a, together with the contour spectrum of the bulk PMMA. A new peak is observed at 287.94 eV, corresponding to a carbon−oxygen bond the bond order of which is greater than 1 and smaller than 2 and hence the bond character is between that of

TABLE 3: A Summary of the C(1s) Core-Level Electron Peaks Obtained at Different Times during the Decomposition Reaction of $Co_2(CO)_8$ in a Solution Containing PMMA

reaction time (h)	peak position (eV)	peak height (N_E/E)
2	287.94	0.46
5	287.94	1.71
10	287.94	2.23
15	287.94	3.07

a carbonyl and a carbon−oxygen single bond.[54,58−61] A summary of the C(1s) core level peaks obtained at different reaction times is given in Table 3, and the increase in the height of the 287.94 eV peak is plotted as a function of time and shown in Figure 7b. The intensity of the new peak increases sharply after the end of the induction period discussed earlier, but stabilizes after ∼10 h. This is in good agreement with the slowing rate of growth of the cobalt oxide nanoclusters, as evidenced by the slower increase in the intensity of the 883 cm^{-1} absorption band shown in Figure 4b. The most striking features of the XPS spectra are the dramatic decrease in the relative intensity of the carbonyl carbon atoms and a considerable increase in the carbons associated with the new peak. The peak generated by carbon atoms singly bonded to oxygen does not seem to be affected by the interaction of PMMA with the cobalt oxide nanoclusters. These observations imply two main conclusions: (a) there has been an extensive reaction of the polymer with the surface of the cobalt oxide nanocluster and (b) there may be more than one single mode of bonding between the PMMA and the surface. The bonding may occur either via the interaction of the carboxylate ion with the cobalt oxide, in which case only one cobalt center per functional group will be involved, or via the separate interaction of each oxygen atom in the carboxylate ion, in which case two cobalt centers per functional group will be involved, as shown:[27,54,62,63]

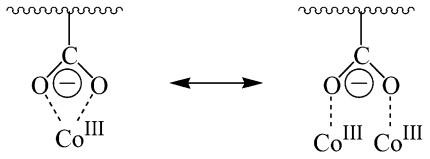

The XPS spectra do not provide sufficient information to distinguish between the two bonding possibilities. The XPS spectra of the corresponding O(1s) core electrons are not shown because they could not be used for the analysis of the reaction mechanism. The bulk PMMA samples generated two O(1s) core electron peaks, corresponding to the carbonyl oxygen and the methoxy oxygen. However, the O(1s) core electron peaks for bare cobalt oxide nanoclusters could not be used as the appropriate baseline for the oxygen peaks originating from the surface because the in situ synthesis of cobalt oxide clusters in the absence of PMMA produces large cobalt oxide aggregates and hence their surface cannot be reliably compared to the bare surface of smaller cobalt oxides, such as those formed in the presence of PMMA. Moreover, even if one would assume similar surface properties for large and small cobalt oxide particles, there is still an insurmountable difficulty in applying surface-sensitive techniques to these particulate systems that will allow the identification of surface-layer cobalt oxide molecules versus inner-layer cobalt oxide molecules.

4. Summary

The intent of the work presented in this paper was to decouple the various contributions embedded in the kinetic information obtained during the synthesis of cobalt oxide nanoclusters stabilized by PMMA chains. Unlike traditional kinetic studies, in which the determination of the precursor decomposition reaction rate is assumed to be representative of the overall cobalt oxide formation rate, we have shown here that there are several crucial steps in the nanoparticle aggregation process and that the traditional assumptions regarding the dynamics of the process are not correct. The formation of cobalt oxide nanoparticles with an average size above the detection threshold of dynamic light scattering (∼3 nm) and TEM (∼2−3 nm) does not mirror the decomposition of the precursor during the same time frame. Moreover, the stabilization process, that is, the adsorption of the polymer chains onto the nanocluster surface, is shown to occur in the later stages of the aggregation, as is evidenced by the common and parallel induction period observed in the formation of the cobalt oxide nanoclusters and the transformations that occur in the ester functional groups of PMMA. It is therefore clear that the aggregation and stabilizations processes occur only after the reactive metallic fragments, that is, metallomers, have reached a critical size and a distinct surface structure.

Acknowledgment. We thank the Surface Science Center at the University of Minnesota and its director, Dr. Raul Carreta, for assistance with the XPS measurements. This work is supported by a University of Minnesota Faculty Research Award and by the Georgia Tech Research Institute Equipment Grant (both to R. Tannenbaum).

References and Notes

(1) Martin, T. P. *Solid State Ionics* **2000**, *131*(1), 3−12.
(2) Klaubunde, K. J.; Tanaka, Y. *J. Mol. Catal.* **1983**, *21*, 57.
(3) Kanai, H.; Tan, B. J.; Klaubunde, K. J. *Langmuir* **1986**, *2* (6), 760.
(4) Bockstaller, M.; Kolb, R.; Thomas, E. L. *Adv. Mater.* **2001**, *13* (23), 1783−1786.
(5) Zhao, S.; Wang, S.; Ye, H. *J. Phys. Soc. Jpn.* **2001**, *70* (10), 2953−2957.
(6) Tannenbaum, R.; Reich, S.; Flenniken, C. L.; Goldberg, E. P. *Adv. Mater.* **2002**, *14* (19), 1402−1405.
(7) Tannenbaum, R.; Flenniken, C. L.; Goldberg, E. P. *J. Polym. Sci., Polym. Phys. Ed.* **1987**, *25*, 1341.
(8) Tannenbaum, R.; Flenniken, C. L.; Goldberg, E. P. *J. Polym. Sci., Polym. Phys. Ed.* **1990**, *28*, 2421.
(9) Tannenbaum, R. *Langmuir* **1997**, *13* (19), 5056 and pertinent references therein.
(10) Heck, R. F.; Breslow, D. S. *J. Am. Chem. Soc.* **1961**, *83*, 4023.
(11) Ungváry, F.; Markó, L. *J. Organomet. Chem.* **1969**, *20*, 205.
(12) Werner, P.; Ault, B. S.; Orchin, M. *J. Organomet. Chem.* **1978**, *162*, 189−194.
(13) LaMer, V. K.; Dinegar, R. H. *J. Am. Chem. Soc.* **1950**, *72*, 4847.
(14) LaMer, V. K. *Ind. Eng. Chem.* **1952**, *44*, 1270.
(15) Smoluchowsky, M. V. *Z. Phys. Chem.* **1917**, *92*, 129.
(16) McLeod, J. B. Q. *J. Math. Oxford (2)* **1962**, *13*, 119.
(17) Ziff, R. M. *J. Stat. Phys.* **1980**, *23*, 241.
(18) Leyvraz, F.; Tschudi, H. R. *J. Phys. A: Math. Gen.* **1982**, *15*, 1951.
(19) Rotstein, H. G.; Novick-Cohen, A.; Tannenbaum, R. *J. Stat. Phys.* **1998**, *90*, 119.
(20) Bird, R. B.; Curtis, C. F.; Hassager, O.; Armstrong, R. C. *Dynamics of Polymeric Liquids: Vol. 2, Kinetic Theory*; Wiley: NewYork, 1987.
(21) Tang, J. G.; Hu, K.; Liu, H. Y.; Guo, D.; Wu, R. J. *J. Appl. Polym. Sci.* **2000**, *76*, 1857−1864.
(22) For example: (a) Zanchet, D.; Hall, B. D.; Ugarte, D. *J. Phys. Chem. B* **2000**, *104* (47), 11013−11018. (b) Whaley, S. R.; English, D. S.; Hu, E. L.; Barbara, P. F.; Belcher, A. M. *Nature* **2000**, *405*, 665−668. (c) Ahmadi, T. S.; Wang, Z. L.; Green, T. C.; Henglein, A.; El-Sayed, M. A. *Science* **1996**, *272*, 1924−1925. (e) Petroski, J. M.; Wang, Z. L.; Green, T. C.; El-Sayed, M. A. *J. Phys. Chem. B* **1998**, *102*, 3316−3320. (f) Wang, Z. L.; Mohamed, M. B.; Link, S.; El-Sayed, M. A. *Surf. Sci.* **1999**, *440*, L809−L814. (g) Bradley, J. S.; Tesche, B.; Busser, W.; Maase, M.; Reetz, M. T. *J. Am. Chem. Soc.* **2000**, *122*, 4631−4636. (h) Wang, Z. L.; Gao, R. P.; Nikoobakht, B.; El-Sayed, M. A. *J. Phys. Chem. B* **2000**, *104*, 5417−5420. (i) Link, S.; Burda, C.; Nikoobakht, B.; El-Sayed, M. A. *J. Phys. Chem. B* **2000**, *104*, 6152−6163.

(23) Watzky, M. A.; Finke, R. G. *J. Am. Chem Soc.* **1997**, *119*, 10382−10400.
(24) Özkar, S.; Finke, R. G. *J. Am. Chem. Soc*. **2002**, *124* (20), 5796−5810.
(25) Widegren, J. A.; Aiken, J. D., III; Özkar, S.; Finke, R. G. *Chem. Mater*. **2001**, *13* (2), 312−324.
(26) Biffis, A.; D′Archivio, A. A.; Jerabek, K.; Schmid, G.; Corain, B. *Adv. Mater.* **2000**, *12* (24), 1909−1912.
(27) Rotstein, H. G.; Tannenbaum, R. *J. Phys. Chem. B* **2002**, *106* (1), 146−151.
(28) Tadd, E.; Bradley, J.; Tannenbaum, R. *Langmuir* **2002**, *18* (6), 2378−2384.
(29) Spatz, J. P.; Mössmer, S.; Hartmann, C.; Möller, M.; Herzog, T.; Krieger, M.; Boyen, H.-G.; Ziemann, P.; Kabius, B. *Langmuir* **2000**, *16*, 407−415.
(30) Tsivline, D.; Stepanyuk, V. S.; Levanov, N.; Hergert, W.; Katsnelson, A. A. *Comput. Phys. Commun.* **1999**, *121*, 747.
(31) Dan, N. *Langmuir* **2000**, *16* (8), 4045.
(32) Tadd, E.; Zeno, A.; Zubris, M.; Dan, N.; Tannenbaum, R. *Macromolecules* **2003**, appeared on the Web (ASAP) on 7/29/03.
(33) Flory, P. J.; Fox, T. G. *J. Am. Chem. Soc*. **1951**, *73*, 1904.
(34) Flory, P. J. *Principles of Polymer Chemistry*; Cornell University Press: Ithaca, New York, 1953.
(35) Graessley, W. W. *Adv. Polym. Sci.* **1974**, *16*, 1.
(36) deGennes, P. G. *Scaling Concepts in Polymer Physics*; Cornell University Press: Ithaca, New York, 1979.
(37) Reetz, M. T. W.; Helbig, S. A.; Quaiser, U.; Stimming, N.; Breuer, R.; Vogel *Science* **1995**, *267*, 367.
(38) Hariharan, R.; Russell, W. B. *Langmuir* **1998**, *14* (25), 7104.
(39) Reich, S.; Goldberg, E. P. *J. Polym. Sci., Polym. Phys. Ed*. **1983**, *21* (6), 869−879.
(40) Griffiths, C. H.; O'Horo, M. P.; Smith, T. W. *J. Appl. Phys*. **1979**, *50* (11), 7108−7115.
(41) Rotstein, H.; Tannenbaum, R. In *Synthesis, Functionalization and Surface Treatment of Nanoparticles*; Baraton, M.-I., Ed.; Advances in Nanoscale Materials and Nanotechnology Book Series; American Scientific Publishers: Stevenson Ranch, CA, 2003; pp 103−126.
(42) Duevel, R. V.; Corn, R. M. *Anal. Chem.* **1992**, *64*, 337.
(43) Wang, B. *Spectroscopy* **1997**, *12* (1), 30.
(44) Ungváry, F.; Markó, L. *J. Organomet. Chem.* **1974**, *71*, 283.
(45) Bor, G.; Dietler, U. K. *J. Organomet. Chem.* **1980**, *191*, 295.
(46) Bor, G.; Dietler, U. K.; Noack, K. *J. Chem. Soc., Chem. Commun*. **1976**, 914.
(47) Noack, K. *Helv. Chim. Acta* **1962**, *45*, 1847 and all pertinent references therein.
(48) Braterman, P. S. *Metal Carbonyl Spectra*; Academic Press: New York, 1975.
(49) Uzunova, E. L.; St. Nikolov, G.; Mikosch, H. *J. Phys. Chem. A* **2002**, *106* (16), 4104−4114.
(50) Werner, P.; Ault, B. S.; Orchin, M. *J. Organomet. Chem.* **1978**, *162*, 189−194.
(51) Konstadinidis, K.; Thakkar, B.; Chakraborty, A.; Potts, L. W.; Tannenbaum, R.; Tirrell, M.; Evans, J. F. *Langmuir* **1992**, *8* (5), 1307−1317.
(52) Allara, D. L. *Polym. Sci. Technol*. **1980**, *12B*, 751.
(53) Mallik, R. R.; Pritchard, R. G.; Horley, C. C. *Polymer* **1985**, *26*, 551.
(54) Tannenbaum, R.; Hakanson, C.; Zeno, A.; Tirrell, M. *Langmuir* **2002**, *18* (14), 5592−5599.
(55) Clark, D. T.; Thomas, H. R. *J. Polym. Sci., Polym. Chem. Ed.* **1971**, *14*, 1701.
(56) Dilks, A. In *Electron Spectroscopy: Theory, Techniques and Applications*; Brundle, C. R., Parker, A. D., Eds.; Academic Press: 1981; Vol. 4, p 277.
(57) Riggs, W. M.; Parker, M. J. In *Methods of Surface Analysis*; Czandera, A. W., Ed.; Elsevier Scientific: 1975; p 103.
(58) Bartha, J. W.; Hahn, P. O.; LeGoues, F. K.; Ho, P. S. *J. Vac. Sci. Technol.* **1985**, *A3*, 1390.
(59) Jordan, J. L.; Sanda, P. N.; Morar, J. F.; Kovac, C. A.; Himpsel, F. J.; Pollak, R. A. *J. Vac. Sci. Technol.* **1986**, *A4*, 1046.
(60) Nuzzo, R. G.; Wong, Y.-H.; Schwartz, G. P. *Langmuir* **1987**, *3* (6), 1136−1140.
(61) Atanasoska, Lj.; Anderson, S. G.; Meyer, H. M., III.; Weaver, J. H. *Vacuum* **1990**, *40* (1−2), 91−94.
(62) Burkstrand, J. M. *J. Appl. Phys.* **1981**, *52* (7), 4795.
(63) DeKoven, B. M.; Hagans, P. L. *J. Appl. Surf. Sci.* **1986**, *27*, 199.